

Available at [www.sciencedirect.com](http://www.sciencedirect.com)

ScienceDirect

journal homepage: [www.elsevier.com/locate/carbon](http://www.elsevier.com/locate/carbon)

# Template growth of porous graphene microspheres on layered double oxide catalysts and their applications in lithium–sulfur batteries



Jia-Le Shi <sup>a</sup>, Hong-Jie Peng <sup>a</sup>, Lin Zhu <sup>a,b</sup>, Wancheng Zhu <sup>b</sup>, Qiang Zhang <sup>a,\*</sup>

<sup>a</sup> Beijing Key Laboratory of Green Chemical Reaction Engineering and Technology, Department of Chemical Engineering, Tsinghua University, Beijing 100084, China

<sup>b</sup> Department of Chemical Engineering, Qufu Normal University, Shandong 273165, China

## ARTICLE INFO

### Article history:

Received 3 January 2015

Accepted 11 March 2015

Available online 17 March 2015

## ABSTRACT

The wise integration of individual two-dimensional graphene nanosheets into three-dimensional (3D) macroscopic architectures is essential for full exploration of their potential applications in electrochemical energy storage. Graphene microspheres (GMSs) with hierarchical porous architectures and high 3D electrical conductivities are highly expected to be the host carbon to accommodate sulfur cathode for lithium–sulfur batteries. Herein we reported the direct synthesis of GMSs assembled by 3D interconnected graphene with hierarchical pores by template chemical vapor deposition (CVD) on layered double oxide (LDO) microspheres. The LDO templates were derived from conformally calcined layered double hydroxide microspheres produced by spray drying. After methane-CVD, graphene was catalytically grown on LDO templates. Subsequent routine chemical etching of the LDO templates enabled as-obtained GMSs with a large diameter of ca. 11  $\mu\text{m}$  and a high surface area of 1275  $\text{m}^2 \text{g}^{-1}$ . The GMS was employed as carbon scaffold to accommodate sulfur for rechargeable lithium–sulfur batteries. An initial areal discharge capacity of 2.67  $\text{mAh cm}^{-2}$  was obtained at a current density of 0.83  $\text{mA cm}^{-2}$  on flexible GMS paper electrode with an areal sulfur loading of 2.5  $\text{mg cm}^{-2}$ .

© 2015 Elsevier Ltd. All rights reserved.

## 1. Introduction

Carbon materials have been extensively utilized in various electrochemical energy storage arouse by their diverse micro-/nanoarchitectures and extraordinary properties of covalent bonding [1]. Particularly, porous carbon obtained by organic casting methods on hard/soft templates afford abundant ion channels and very high surface area ( $>800 \text{ m}^2 \text{g}^{-1}$  in most cases) but poor electrical conductivity (less than  $1 \text{ S m}^{-1}$ ). The  $\text{sp}^2$  carbon (e.g. graphene, carbon

nanotubes (CNTs)) delivers outstanding mechanical strength and very high electrical conductivity (larger than  $100 \text{ S m}^{-1}$ ) but normally limited external accessible surface area due to its poor macroscopic dispersion. If the  $\text{sp}^2$  carbon is rationally integrated into monolithic porous architectures with high three-dimensional (3D) electrical conductivity, their bulk applications will be further extended [2–5]. The involving complex material chemistry can also be revealed to fully demonstrate their potential properties in device scale.

\* Corresponding author: Fax: +86 10 62772051.

E-mail address: [zhang-qiang@mails.tsinghua.edu.cn](mailto:zhang-qiang@mails.tsinghua.edu.cn) (Q. Zhang).

<http://dx.doi.org/10.1016/j.carbon.2015.03.031>

0008-6223/© 2015 Elsevier Ltd. All rights reserved.

Spherical particles are widely accepted by material industries for batteries and supercapacitors. Active materials with a spherical shape are favorable to minimize viscous effects, increase integrating homogeneity, and display better electrochemical performance due to their shorter but more uniform diffusion pathway as well as better flow characteristics against other irregular anisotropic particles. Carbon spheres are highly concerned for recently electrochemical energy storage. For instance, the use of silica hard templates as well as the extensive Stöber method [6] to prepare monodisperse carbonaceous nanospheres has been reported. Carbon spheres derived from resin with hierarchical porous nanostructures were emerging novel nanocarbon for advanced supercapacitors [7], lithium ion batteries [8], lithium–sulfur batteries [9], as well as lithium–selenium batteries [10]. However, the graphitic domains in these carbonaceous nanospheres were always very small and their electrical conductivities were expected to be enhanced for better device performance.

Graphene, two-dimensional (2D)  $sp^2$  carbon allotrope, has been strongly considered into macroscopic multi-dimensional assemblies as fibers, spheres, foam, sponges, and films toward multi-functional properties and vast applications [11,12]. Among a family of macroscopic graphene architectures, graphene spheres were highly concerned for their unique structures and emerging applications in energy storage, water treatment, environmental protection, composites, as well as biosensors [13–18]. For instance, Chen and co-workers reported the electro-spray-assisted self-assembly of erythrocyte-like graphene microspheres with perfect exterior doughnut shape and interior porous network for rapid and recyclable removal of oil and toxic organic solvents from water [13]. Wang and co-workers fabricated porous pyrolyzed polyacrylonitrile–sulfur@graphene nanosheet with a size of 1–10  $\mu\text{m}$  by spray drying with a very impressive performance for lithium–sulfur batteries [14]. Yan and co-workers firstly reported the facile synthesis of nitrogen-doped graphene microspheres via poly(methylmethacrylate)-assisted chemical vapor deposition (CVD) graphene growth on nickel microspheres and following urea-assisted hydrothermal reaction at 200 °C for nitrogen doping with a diameter of 5–10  $\mu\text{m}$  for electrochemical biosensors of glucose oxidase [15]. 5–10  $\mu\text{m}$  porous nitrogen/sulfur-codoped graphene-like microspheres were fabricated using nickel microspherical templates with poly(vinylpyrrolidone) carbon sources and  $(\text{NH}_4)_2\text{S}_2\text{O}_8$  nitrogen/sulfur precursors for lithium ion batteries with superior capacity and cycling stability [16]. Jiang et al. explored the nitrogen-doped holey graphene hollow microspheres of ca. 200 nm through template reduction of graphene oxide on silica spheres for high rate anode materials of lithium ion batteries [17]. The use of spray-assisted deep-frying [18] and spherical hard templates (e.g. polystyrene [19], poly(methylmethacrylate) [20]) were efficient routes to assemble of graphene oxide into hollow graphene microspheres with unexpected properties and applications. Very recently, we proposed a mesoscale approach to fabricate graphene nanoshells with quite small diameters of 10–30 nm through a catalytic self-limited assembly of nanographene on in situ formed nanoparticles for high-rate lithium–sulfur batteries [21]. If the graphene microspheres (GMSs), especially with large surface area and high 3D electrical conductivity, could

be bulk synthesized in a controllable manner, the ubiquitous properties and emerging applications of graphene monolith would be fully demonstrated, and the mechanistic insight into the synthesis of macroscopic graphene assembly could be detailed explored.

In this contribution, we reported the direct synthesis of GMSs assembled by 3D interconnected graphene with hierarchical pores by template CVD growth on layered double oxide (LDO) microspheres. The reason we selected LDO as templates was aroused from their catalytic activities for template deposition of graphene as well as high thermal stability during high-temperature CVD of  $\text{CH}_4$  [22]. The compositions and topologies of LDO templates can be delicately mediated in a wide range, thus affording high tunability of graphene template growth. As illustrated in Fig. 1, spherical porous layered double hydroxide (LDH) assemblies were employed as the template precursors and then conformally calcined to obtain LDO microsphere templates. Graphene was organized and casted on the LDO catalysts through a high-temperature CVD of  $\text{CH}_4$  while purified GMSs were obtained after facile chemical etching. The GMSs reported herein inherited a self-supporting nature from template microspheres and composed of 3D interconnected graphene nanocages and nanosheets. Lithium–sulfur batteries, an emerging electrochemical energy storage system with high theoretical energy density of 2567  $\text{Wh kg}^{-1}$  held great practical promise while, however, were hindered by poor utilization of active materials, low efficiency, and undesirable service life [23–25]. Herein lithium–sulfur batteries were considered as a probe device to evaluate the performance of GMSs. The GMSs were

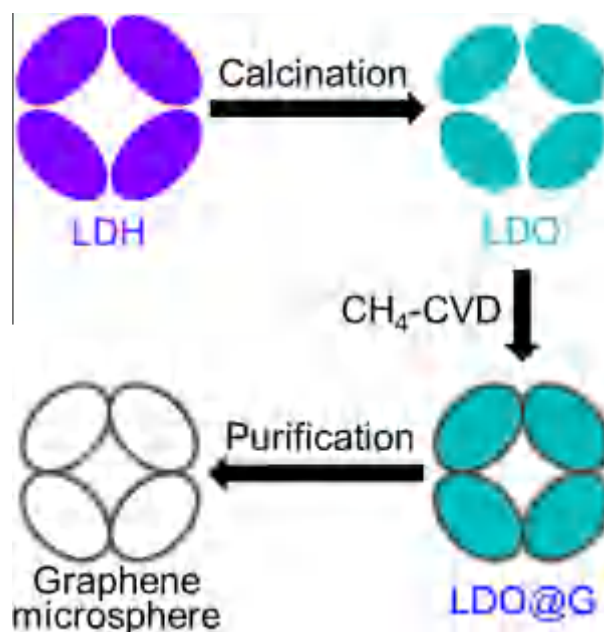


Fig. 1 – Scheme for the synthesis of GMS. A porous microsphere derived from the calcination of spherical LDH assembly was used as the template to cast graphene through CVD. The template was removed by chemical etching, whereas the graphene microsphere was preserved due to the 3D interconnected graphene networks. (A color version of this figure can be viewed online.)

found to be an effective and efficient cathode scaffold for sulfur with superior lithium ion storage performance.

## 2. Experimental

### 2.1. Preparation of graphene microspheres

Nanosized MgAl-LDHs (molar ratio Mg:Al = 2:1) were prepared by a method involving separate nucleation and aging step [26]. The final precipitate was filtered, washed thoroughly until pH = 7.0, and re-dispersed with deionized water to form the precursor slurry. Subsequent spray drying process was conducted to form  $[\text{Mg}_2\text{Al}(\text{OH})_6](\text{CO}_3)_{0.5}\text{mH}_2\text{O}$  (MgAl-CO<sub>3</sub>-LDH) microspheres [27]. The LDO templates were obtained by calcination of MgAl-LDH microspheres at a rate of 30 °C min<sup>-1</sup> to 950 °C under flowing Ar (200 mL min<sup>-1</sup>) and kept at that temperature for 1.0 h in a horizontal quartz tube reactor. Afterwards, template CVD growth of graphene was started by introduction of CH<sub>4</sub> (600 mL min<sup>-1</sup>). The reaction was maintained for 10 min before the furnace was cooled to room temperature under Ar protection. The as-grown raw products were purified by NaOH (15.0 mol L<sup>-1</sup>) aqueous solution at 180 °C for 12.0 h and HCl (5.0 mol L<sup>-1</sup>) aqueous solution at 80 °C for 12.0 h sequentially to remove the MgAl-LDO templates. The GMSs were collected after the product was filtered, washed, and freeze dried.

### 2.2. Fabrication of GMS-S/CNT flexible cathode

The GMS-S composite was prepared by a facile melt-diffusion strategy. Typically, the mixture containing 20 wt% GMSs and 80 wt% sulfur powder was strongly grinded in an agate mortar for 10 min. To completely incorporate the sulfur into the micro-/mesopores of the GMSs, the as-obtained mixture was then placed in a sealed quartz bottle at 155 °C for 4.0 h. The flexible GMS-S electrode was fabricated by a shearing dispersion-filtration method. Super-long aligned CNTs with a length of ca. 4.0 mm and a diameter of 30–40 nm were fabricated by floating catalyst CVD [28]. 12.0 mg of super-long CNTs were dispersed in sulfur-saturated ethanol solution and kept shearing for 3.0 min in an ice bath. 24.0 mg of GMS-S composite materials was added to above-mentioned suspension and further sheared for another 1.0 min. The whole dispersion was filtrated to obtain a flexible paper electrode with an areal sulfur loading of 2.5 mg cm<sup>-2</sup>. After that, the film was dried at 60 °C for 12.0 h. 13.0 mm-diameter disks were punched as the working electrodes for lithium-sulfur cells.

### 2.3. Structure characterizations

The morphology of samples were characterized by a JEM 2010 high solution transmission electron microscope (TEM) at 120.0 kV and a JSM 7401F field-emission scanning electron microscope (SEM) at 3.0 kV. XRD patterns were recorded on a Bruker D8 Advance diffractometer equipped with a Cu-K<sub>α</sub> radiation source. Raman spectra were obtained with a He-Ne laser excitation at 633 nm using LabRAM HR800 Raman spectrophotometer (Horiba Jobin Yvon). Thermogravimetric

analysis (TGA) was performed by the Mettler Toledo TGA/DSC1 STAR<sup>e</sup> system with a temperature ramp rate of 20 °C min<sup>-1</sup>. N<sub>2</sub> isotherms were obtained at -196 °C (77 K) with an Autosorb-IQ<sub>2</sub>-MP-C system (Quantachrome). The specific surface area (SSA) was determined by the Brunauer-Emmett-Teller (BET) method. The pore size distribution was calculated using the density functional theory (DFT) method from the adsorption branches of the isotherms. The sample was degassed at the right temperature for 10.0 h to avoid the influence of impurities (a degas temperature of 30 °C for LDH and GMS-S and 300 °C for LDO, LDO@G, and GMS) before N<sub>2</sub> physisorption measurements. The four-probe method was performed to determine the powder conductivity of the GMSs, which were compressed into a dense disk with 13.0 mm-diameter under a pressure of 8.0 MPa.

### 2.4. Electrochemical performance evaluation

The standard 2025 coin-type cells were employed for electrochemical performance evaluation of flexible GMS-S electrodes. The electrolyte was 1.0 mol L<sup>-1</sup> lithium bis(trifluoromethanesulfonyl)imide in dimethyl ether and 1,3-dioxolane (volume ratio 1:1). 1.0-mm-thick lithium metal foil was applied as the anode and the Celgard 2400 membranes were acted as the separator. The lithium-sulfur cells were assembled in an argon-filled glove-box with 50 lL electrolyte. The cyclic performance was collected by Neware multi-channel battery cycler within a voltage window of 1.6–2.8 V.

## 3. Results and discussion

### 3.1. Template growth of the GMSs

MgAl-LDO microspheres obtained by the conformal calcination of spherical MgAl-LDH assemblies were adopted as hierarchical templates for the CVD growth of GMSs. LDHs are a class of ionic lamellar compounds composed of positively charged brucite-like layers with interlayered charge-balancing anions and solvent molecules [29–31]. Spray-dried LDH microspheres showed a diameter of ca. 111 nm and revealed sub-units of small nanoparticles (Fig. 2a). Interconnected macroporous structure was constructed by LDH nanoparticles (Fig. S1a), which could facilitate mass transfer of carbon sources during CVD growth. The lateral size of LDH nanoplatelets was less than 100 nm while the thickness was around 20 nm (Fig. 2b). The high-resolution TEM image of LDH side view showed a d-spacing of 0.76 nm, corresponding to the basal spacing of (003) crystal plane of MgAl-CO<sub>3</sub>-LDH (the inset figure of Fig. 2b) [32]. The MgAl-CO<sub>3</sub>-LDHs gradually underwent removal of interlayer H<sub>2</sub>O molecules, dehydroxylation of the layers, decomposition of the interlayer CO<sub>3</sub><sup>2-</sup>, and formation of MgAl<sub>2</sub>O<sub>4</sub> spinel phase during the calcination (Fig. S1b). The LDO residual was ca. 56.6 wt% of LDH precursor. After calcination at 950 °C for 1.0 h, the as-obtained LDO microspheres were conformally preserved without obvious change of morphology and size (Fig. 2c). With the introduction of CH<sub>4</sub>, hydrocarbon molecules decomposed on the surface of LDO at high temperature

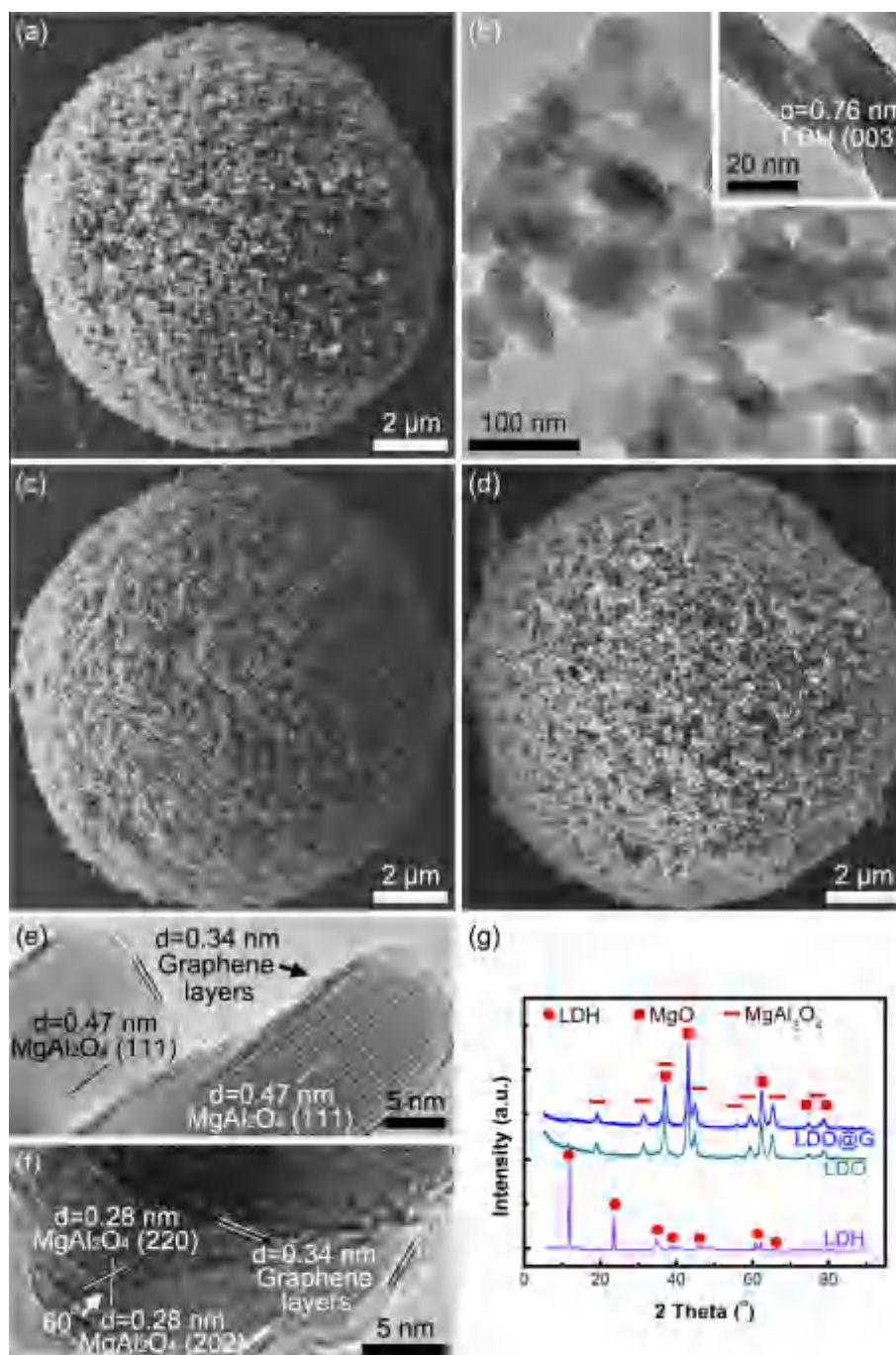


Fig. 2 – Structure evolution of the templates for graphene deposition. SEM image of (a) the spray-dried LDH microspheres; TEM images of (b) the LDH sub-units, side view of MgAl-CO<sub>3</sub>-LDH (inset); SEM images of (c) calcined LDO and (d) LDO@G microspheres; (e and f) TEM images of graphene casted onto LDO nanoparticles; (g) XRD patterns of the LDH, LDO, and LDO@G microspheres. (A color version of this figure can be viewed online.)

of 950 °C and carbon atoms recombined into graphene lattice. However, the spherical assembly was still well maintained in the macroscopic scale (Fig. 2d). High-resolution TEM images further indicated the microscale texture that thin-layer graphene was deposited and tightly adhered to the catalytic surface of LDO nanocrystals (Fig. 2e and f). Impeccable alignment of adjacent (111) plane with a d-spacing of 0.47 nm indicated high crystalline degree of MgAl<sub>2</sub>O<sub>4</sub> spinel

crystals while an individual crystal domain still remained small size, which rendered high curvature of deposited graphene at nanoscale (Fig. 2e). The MgAl<sub>2</sub>O<sub>4</sub> spinel phase was also validated by (220) and (202) planes with a rotation angle of 60° (Fig. 2f). Only 1–2 layer of graphene was detected on LDO. Thus, inherent extraordinary properties were expected to be fully interpreted beyond multi-layer graphene with layer number larger than 4.

Aforementioned phase evolution of LDH to LDO, and to LDO@graphene (LDO@G) was further revealed by powder XRD patterns (Fig. 2g). Pristine LDHs exhibited a series of (001) peaks appearing at low angle, while the hydrotalcite-like MgAl-CO<sub>3</sub>-LDH phase was completely transformed into MgAl-LDO as MgO and MgAl<sub>2</sub>O<sub>4</sub> mixture. Both MgO and MgAl<sub>2</sub>O<sub>4</sub> with an oxygen-terminated surface and high thermal stability were employed as the templates for CVD growth of graphene [33]. The characteristic diffraction peak of graphite at 26.4° was indiscernible for XRD pattern of LDO@G, demonstrating the few-layer nature of deposited graphene in macroscopic scale. All of the XRD patterns were in good accordance with high resolution TEM images. The N<sub>2</sub> isotherms showed few difference among LDH, LDO, and LDO@G microspheres, suggesting similar macroporous structure and less sintering of oxides (Fig. S2). The conformal transformation of LDH precursors and LDO templates was the prerequisite for direct synthesis of GMSs.

### 3.2. Morphology and structural analysis of the GMSs

The LDO templates can be completely removed by the rigid NaOH and HCl treatment. The as-obtained GMSs exhibited a similar microsphere morphology and a diameter of ca. 111 nm, all of which were conformally inherited from LDH

precursors and LDO templates (Figs. 3a and S3a). The SEM image of GMS in an enlarged cross-section region clearly revealed the porous structure inside the microsphere (Fig. S3b). The GMSs were constituted of interconnected graphene networks at extended dimension. There were abundant mesopores and macropores contributed by voids induced by the removal of LDOs and original interspaces between template building blocks, respectively (Fig. 3b). Interior nanographene was highly curved and thus, prevented the common stacking issue. Few-layer feature of as-deposited graphene sheath on LDO was expected to be preserved. Interconnected graphene was casted from LDO templates (Fig. 3c). The interconnection was attributed to adjacent MgO and MgAl<sub>2</sub>O<sub>4</sub> template building blocks. This was similar to the template growth of unstacked double layered template graphene [22] and graphene nanocages [34]. Most graphene nanocages showed an interior size of 20–50 nm, contributing to the majority of mesopore volume while large macropores were inherited from the interspace of pristine LDO nanoflakes. 1–2 layer of graphene was observed without any physical support after template removal (inset of Fig. 3c), indicating no obvious re-stacking during aqueous treatment. This was mainly attributed to the curved nature of nanographene derived from template nanoparticles. A graphene yield of 0.1 g<sub>G</sub> g<sub>LDO</sub><sup>-1</sup> was obtained on the LDO template.

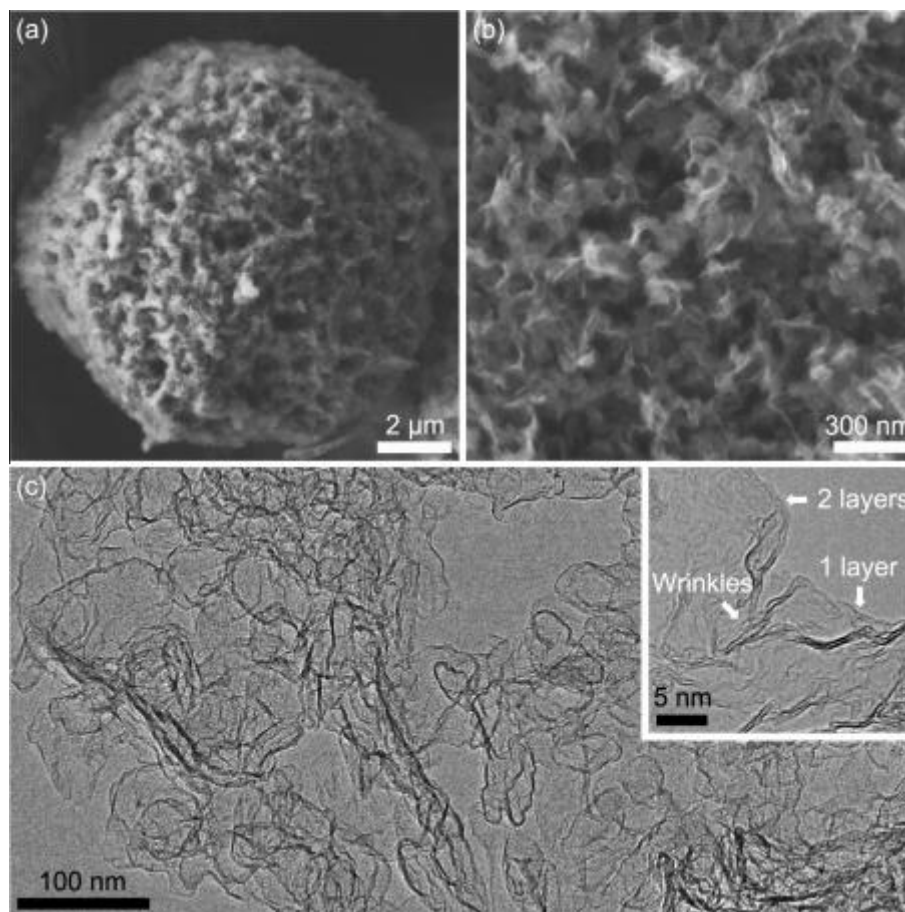


Fig. 3 – Nanostructure of GMSs. SEM images of (a) GMSs and (b) 3D interconnected graphene networks inside GMSs; (c) TEM images of GMSs with interconnected graphene nanocages and few-layer graphene walls of GMSs (inset).

The Raman spectra of GMS samples indicated no significant difference between before and after routine purification (Fig. 4a). A large intensity ratio of D band to G band ( $I_D/I_G$ ) of 1.96 can be obtained for GMSs, indicated high-density defects on the templated graphene grown herein. This is much higher than graphene grown on Cu catalyst with an  $I_D/I_G$  ratio of 0.03–0.2 [35] or graphene grown on MgO (an  $I_D/I_G$  ratio of 1.0) [36] or vermiculite (an  $I_D/I_G$  ratio of 0.94) [37]. The  $N_2$  isotherm of LDO@G showed low adsorption amount until relative pressure ( $P/P_0$ ) reached 0.95 (Fig. 4b). The  $N_2$  were mainly condensed into interconnected macropores of hierarchical LDO@G microspheres. In contrast, GMSs exhibited a sharp increase at region of  $P/P_0 < 0.05$  and a dominant hysteresis loop, indicating a hierarchical micro- and mesoporous structure, respectively. Since the only difference between GMS and LDO@G was removal of LDO templates, the mesopores were derived from the voids of graphene nanocages casted on MgO and  $MgAl_2O_4$  nanocrystals while the micropores could be surface defects induced by chemical etching. Such a hierarchical porous structure was further confirmed by pore size distribution. The LDO@G microspheres had a  $SSA_{BET}$  of  $54 \text{ m}^2 \text{ g}^{-1}$ , while the  $SSA_{BET}$  of GMSs was  $1275 \text{ m}^2 \text{ g}^{-1}$ , which was much higher than routine reduced graphene oxide ( $293\text{--}434 \text{ m}^2 \text{ g}^{-1}$ ) [38] and graphene grown from vermiculite catalyst ( $333 \text{ m}^2 \text{ g}^{-1}$ ) [37]. The TGA profile exhibited a sharp weight loss peak around  $600 \text{ }^\circ\text{C}$  and a total weight loss of ca. 99.98%, indicating the high purity of the purified GMSs (Fig. S4). An electrical conductivity of  $27 \text{ S cm}^{-1}$  can be determined by the four probe method on the compact GMSs, which was ascribed to 3D interconnected graphene scaffolds.

### 3.3. Construction of the GMS-S composites

The lithium–sulfur batteries are strongly considered to be advanced power sources as next-generation rechargeable batteries. However, lithium–sulfur batteries encounter challenges in the aspects of insulative nature of solid products, volume changes during cycling, and complex shuttle of polysulfides for poor stability. In this contribution, together with the high conductivity, large SSA, and excellent porosity derived from 3D graphene scaffolds and interconnected micro-/meso-/macropores, the GMSs were expected to be promising cathode scaffolds to accommodate sulfur for

lithium–sulfur batteries. The GMS-S composite cathodes were fabricated by a facile melt-diffuse method for sulfur accommodation. The cross-section of GMS-S exhibited infiltration of sulfur into the whole spherical assembly (Fig. 5a). Due to the strong confinement of graphene nanocages, sulfur in forms of small nanoparticles was observed to attach on the graphene layers of GMSs (Fig. 5b). As shown in Fig. 5c, the volatilization temperature of total ca. 77.7 wt% sulfur in the GMS-S composites increased from  $160\text{--}270 \text{ }^\circ\text{C}$  of pure sulfur to  $200\text{--}450 \text{ }^\circ\text{C}$ , indicating an effective trapping of sulfur in the porous structure of the GMSs. The sulfur content in GMS-S was not the highest (e.g. 87 wt% sulfur were enveloped in a reduced graphene oxide [39]) but compatible to other graphene hosts reported in published literatures (e.g. solvothermal porous graphene-sulfur of 22 wt% [40],  $H_2S$ -reduced graphene oxide/sulfur of 40 wt% [41], polyacrylonitrile/graphene/sulfur cathode of 47 wt% [42], fibrous hybrid of graphene and sulfur cathode of 59 wt% [43], ‘fish-in-net’ graphene/sulfur cathode of 66 wt% [44], ethylenediamine-functionalized graphene/sulfur cathode of 60–69 wt% [45], ball-milling graphene nanoplatelet-sulfur cathode of 70 wt% [46]). Most of the micro-/mesopores of the GMS are filled with sulfur, as indicated by the markedly decreased pore volume of GMS-S after the incorporation of sulfur (Fig. 5d).

### 3.4. Electrochemical performance of flexible paper cathode

The GMS-S composites were uniformly distributed into super-long CNT scaffolds as flexible electrodes through shearing dispersion-filtration method. The GMS-S/CNT flexible film with a thickness of ca.  $140 \text{ } \mu\text{m}$  exhibited good flexibility (inset of Fig. 6a). The areal sulfur loading amount in the flexible paper electrode reached  $2.5 \text{ mg cm}^{-2}$ , which was higher than the routine blade coating procedure [9,14]. The super-long CNTs were employed as adhesive binders and long range 3D current collectors [47,48], which was an efficient way to demonstrate the potential of novel carbon materials for device with high loading amount.

The flexible GMS-S electrode displayed good rate performance in consideration of high sulfur content and areal loading amount (Fig. 6a). An initial discharge capacity of  $1066 \text{ mAh g}^{-1}$  at  $0.14 \text{ mA cm}^{-2}$  and a high-rate capacity retention of 46.7% at the current density of  $1.35 \text{ mA cm}^{-2}$  were

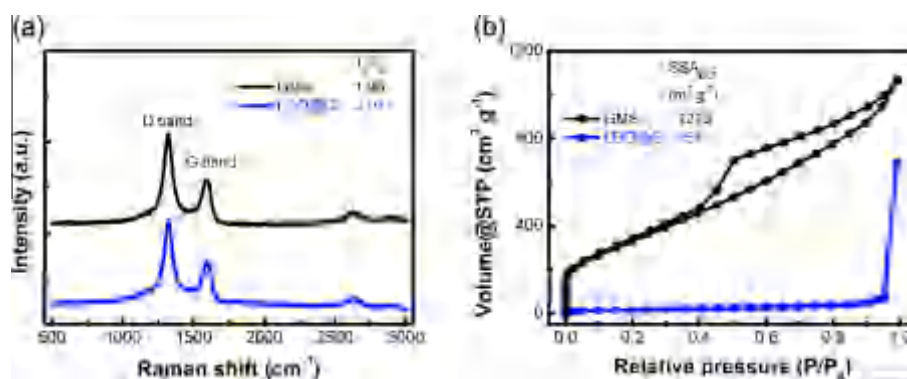


Fig. 4 – (a) Raman spectra and (b)  $N_2$  isotherms of GMSs and LDO@G microspheres. (A color version of this figure can be viewed online.)

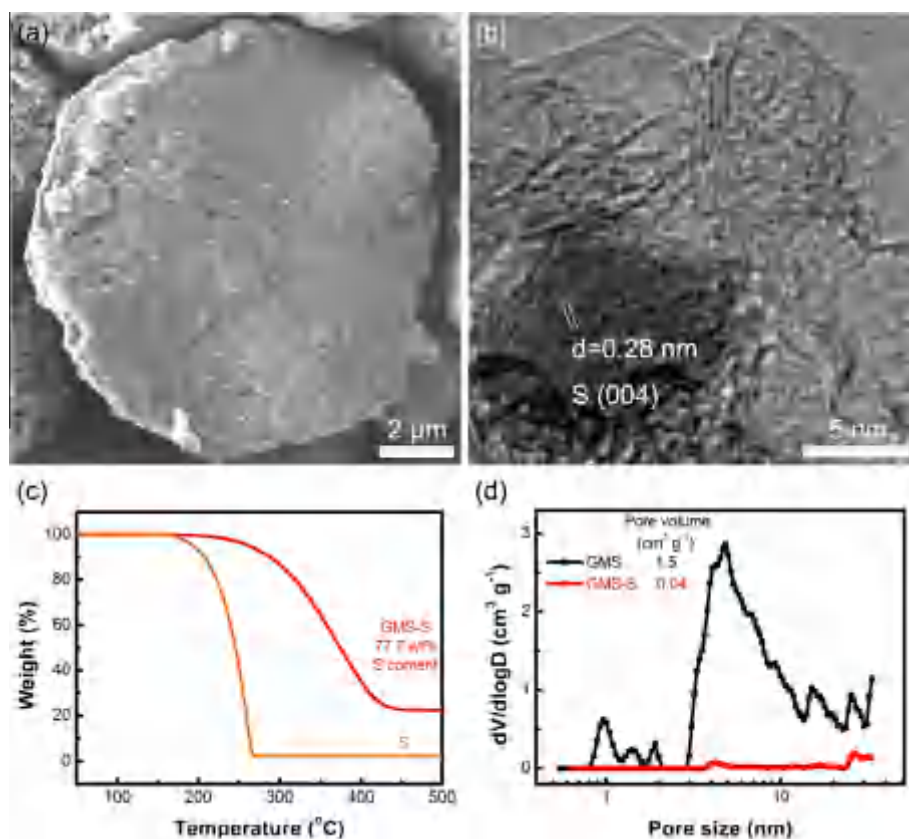


Fig. 5 – Characterization of the GMS-S composites. (a) The cross-sectional SEM image, (b) the high resolution TEM image, (c) the  $N_2$  thermogravimetric profile, and (d) the pore size distribution derived from  $N_2$  isothermal adsorption plot of GMS-S. (A color version of this figure can be viewed online.)

recorded. With the increase of current density, galvanostatic discharge/charge curves of GMS-S flexible electrodes sustained a typical two-plateau profiles except for enhanced polarization (Fig. 6b). The two plateaus corresponded to two-step reduction of sulfur into polysulfides and lithium sulfides while the sluggish kinetics at high rate was attributed from the larger ion diffusion resistance.

Cycling stability was another key aspect limiting the practical use of lithium-sulfur batteries. The GMS-S flexible electrode displayed an initial discharge capacity of  $2.67 \text{ mAh cm}^{-2}$  ( $1068 \text{ mAh g}^{-1}$ ) at  $0.83 \text{ mA cm}^{-2}$  (Fig. 6c). Despite of a relatively high sulfur loading of  $2.5 \text{ mg cm}^{-2}$ , the capacity maintained at  $2.01 \text{ mAh cm}^{-2}$  ( $804 \text{ mAh g}^{-1}$ ) over 80 cycles, corresponding to 75.3% retention of initial capacity. The Coulombic efficiency of the coin cell was above 90.0% in the whole 80 cycles. This discharge capacity was higher than those values recently reported for routine carbon microspheres-S composites cathodes with metal foil current collectors [9,14]. Recently, Wang and co-workers reported a mesoporous carbon-sulfur composite microspheres by combining emulsion polymerization and the evaporation-induced self-assembly process with a sulfur content of 60 wt% and a high sulfur loading of  $5.0 \text{ mg cm}^{-2}$  afforded a reversible capacity of  $740 \text{ mAh g}^{-1}$  after 50 cycles [48]. Kaskel and co-workers presented a highly flexible freestanding carbon-sulfur composite cathode foils containing of 53 wt% sulfur, 27 wt% porous carbon host, 10 wt% CNT conducting agent,

and 10 wt% poly(tetrafluoroethylene) binder afforded a maximal discharge capacity of  $1045 \text{ mAh g}^{-1}$  as well as a high reversible capacity of  $742 \text{ mAh g}^{-1}$  after 160 cycles at a high sulfur loading of  $3.0\text{--}3.2 \text{ mg cm}^{-2}$  [49]. In this contribution, although the sulfur ratio was very high, the sulfur can be utilized in high efficiency and good stability. Thus, GMS can be regarded as a promising carbon host with high areal loading of active materials for lithium-sulfur batteries.

The excellent lithium ion storage performance of the GMS electrode reported herein was attributed to the following aspects: (1) 3D interconnected porous graphene networks for high sulfur capacity, sustaining huge volume change and retaining intimate electrical contact, (2) space confining property of graphene nanocage building blocks to retard severe dissolution of polysulfides, (3) both mechanically and chemically robust CNT scaffolds to form binder-free interconnected electron channels instead of organic binder and metal current collector, improving long-term lifespan with high stability, and (4) the short-range graphene walls of the GMSs and long-range CNT scaffolds served as electron pathways [48–50], the 3D interconnected pores in the GMS particle and among CNTs used as ion channels for rapid transportation in the GMS/CNT composite cathode, consequently, this rendered a 46.7% retention when the current density increased from  $0.14$  to  $1.35 \text{ A cm}^{-2}$ . If other porous long range current collector/binder can be employed, such as graphene foam [51] or 3D porous carbon fiber scaffolds [52,53] were employed,

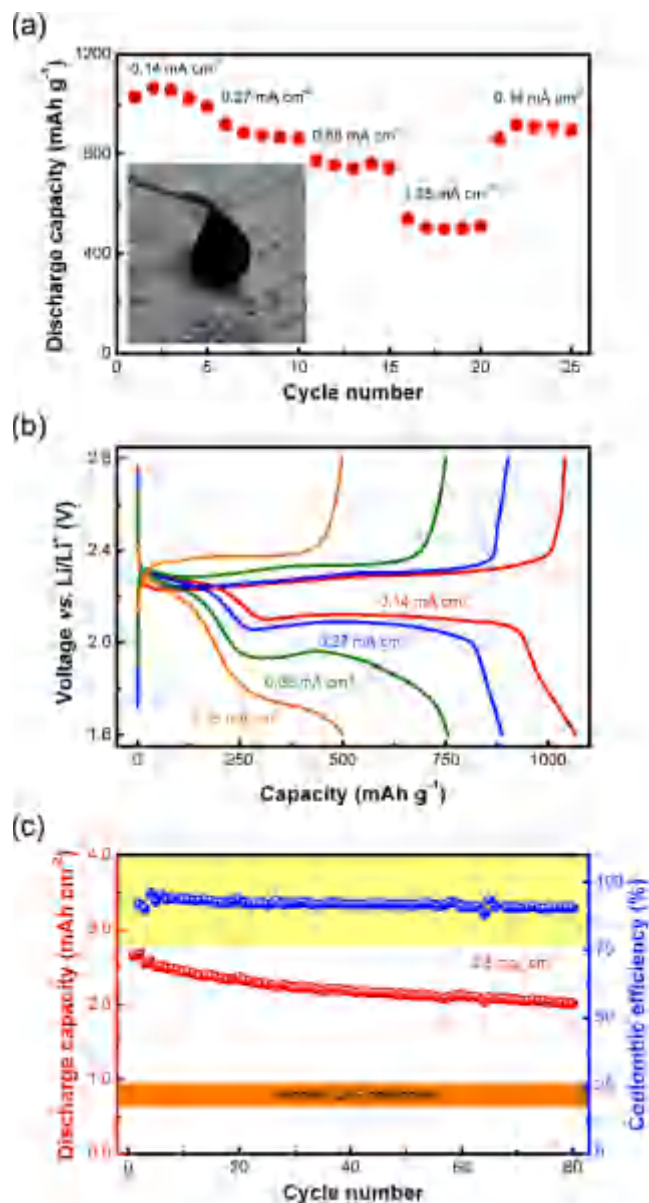


Fig. 6 – Lithium-sulfur battery performance of flexible GMS-S/CNT cathodes. (a) The rate performance, digital image (inset), (b) galvanostatic charge/discharge curves of different current rate, and (c) cycling performance. (A color version of this figure can be viewed online.)

flexible electrode with high areal capacity was highly expected, even the areal loading amount was as high as commercial loading amount of 4–15 mg cm<sup>-2</sup>. The Coulombic efficiency as well as the cycling performance was expected to be improved with the addition of LiNO<sub>3</sub> as anode protectors [54] and ion selective membranes [55,56]. The GMS was expected to be a rational building block to construct high-capacity, high-stability, and high-rate lithium-sulfur batteries.

#### 4. Conclusions

Graphene microspheres assembled by 3D interconnected graphene with hierarchical porous architectures were fabricated

by template CVD growth on spherical LDO assemblies. GMSs with macroscopic dimension possessed a large diameter of ca. 11 μm, a high surface area of 1275 m<sup>2</sup> g<sup>-1</sup>, and a high electrical conductivity of 27 S cm<sup>-1</sup>. The GMSs were employed as the conductive scaffold to encapsulate sulfur for lithium-sulfur batteries. The flexible GMS paper electrode delivered an initial discharge capacity of 1066 mAh g<sup>-1</sup> at 0.14 mA cm<sup>-2</sup> and a capacity retention of 46.7% at the current density of 1.35 mA cm<sup>-2</sup>. With a high sulfur loading of 2.5 mg cm<sup>-2</sup>, an initial discharge capacity of 2.67 mAh cm<sup>-2</sup> at 0.83 mA cm<sup>-2</sup>, and the discharge capacity maintained at 2.01 mAh cm<sup>-2</sup> over 80 cycles, corresponding to 75.3% retention of initial capacity. This was contributed by the 3D interconnected porous graphene networks for high sulfur capacity, sustaining huge volume change and retaining intimate electrical contact, space confining property of graphene nanocage building blocks to retard severe dissolution of polysulfides, as well as the extraordinary mechanically and chemically robust nanocarbon scaffolds. This work offered a novel material platform and mechanistic material chemistry for macroscopic graphene monolithic to fully demonstrate their bulk applications in the area of composites, energy conversion, catalysis, and devices.

#### Acknowledgements

This work was supported by the Natural Scientific Foundation of China (No. 21422604) Tsinghua University Initiative Scientific Research Program (2014z22076), and the National Basic Research Program of China (973 Program 2015CB932500). Thanks discussion from Dr. Jia-Qi Huang, Dr. Meng-Qiang Zhao, Cheng Tang, Gui-Li Tian, Dr. Jianfei Yu, and Dr. Fei Wei for insightful discussion.

#### Appendix A. Supplementary data

Supplementary data associated with this article can be found, in the online version, at <http://dx.doi.org/10.1016/j.carbon.2015.03.031>.

#### REFERENCES

- [1] Su DS, Schloegl R. Nanostructured carbon and carbon nanocomposites for electrochemical energy storage applications. *ChemSusChem* 2010;3:136–68.
- [2] Yan J, Wang Q, Lin CP, Wei T, Fan ZJ. Interconnected frameworks with a sandwiched porous carbon layer/graphene hybrids for supercapacitors with high gravimetric and volumetric performances. *Adv Energy Mater* 2014;4:1400500.
- [3] Peng HJ, Huang JQ, Zhao MQ, Zhang Q, Cheng XB, Liu XY, et al. Nanoarchitected graphene/CNT@porous carbon with extraordinary electrical conductivity and interconnected micro/mesopores for lithium-sulfur batteries. *Adv Funct Mater* 2014;24:2772–81.
- [4] Yang X, Zhang L, Zhang F, Huang Y, Chen YS. Sulfur-infiltrated graphene-based layered porous carbon cathodes for high-performance lithium-sulfur batteries. *ACS Nano* 2014;8:5208–15.

- [5] Li Q, Zhang ZA, Guo ZP, Lai YQ, Zhang K, Li J. Improved cyclability of lithium–sulfur battery cathode using encapsulated sulfur in hollow carbon nanofiber@nitrogen-doped porous carbon core-shell composite. *Carbon* 2014;78:1–9.
- [6] Liu J, Yang TY, Wang DW, Lu GQM, Zhao DY, Qiao SZ. A facile soft-template synthesis of mesoporous polymeric and carbonaceous nanospheres. *Nat Commun* 2013;4:2798.
- [7] Zhang CF, Hatzell KB, Boota M, Dyatkin B, Beidaghi M, Long DH, et al. Highly porous carbon spheres for electrochemical capacitors and capacitive flowable suspension electrodes. *Carbon* 2014;77:155–64.
- [8] Chen TQ, Pan L, Loh TAJ, Chua DHC, Yao YF, Chen Q, et al. Porous nitrogen-doped carbon microspheres as anode materials for lithium ion batteries. *Dalton Trans* 2014;43:14931–5.
- [9] Xu H, Deng Y, Zhao Z, Xu H, Qin X, Chen GH. The superior cycle and rate performance of a novel sulfur cathode by immobilizing sulfur into porous N-doped carbon microspheres. *Chem Commun* 2014;50:10468–70.
- [10] Liu L, Wei Y, Zhang C, Zhang C, Li X, Wang J, et al. Enhanced electrochemical performances of mesoporous carbon microsphere/selenium composites by controlling the pore structure and nitrogen doping. *Electrochim Acta* 2015;153:140–8.
- [11] Hu C, Song L, Zhang Z, Chen N, Feng Z, Qu L. Tailored graphene systems for unconventional applications in energy conversion and storage devices. *Energy Environ Sci* 2015;8:31–54.
- [12] Jiang LL, Fan ZJ. Design of advanced porous graphene materials: from graphene nanomesh to 3D architectures. *Nanoscale* 2014;6:1922–45.
- [13] Tian YY, Wu G, Tian XK, Tao XM, Chen W. Novel erythrocyte-like graphene microspheres with high quality and mass production capability via electrospray assisted self-assembly. *Sci Rep* 2013;3:3327.
- [14] Wang J, Yin L, Jia H, Yu H, He Y, Yang J, et al. Hierarchical sulfur-based cathode materials with long cycle life for rechargeable lithium batteries. *ChemSusChem* 2014;7:563–9.
- [15] Sun D, Yang J, Yan X. Synthesis and electrochemical biosensing properties of hierarchically porous nitrogen-doped graphene microspheres. *ChemElectroChem* 2015;2:348–53.
- [16] Sun D, Yang J, Yan X. Hierarchically porous and nitrogen, sulfur-codoped graphene-like microspheres as a high capacity anode for lithium ion batteries. *Chem Commun* 2015;51:2134–7.
- [17] Jiang ZJ, Jiang ZQ. Fabrication of nitrogen-doped holey graphene hollow microspheres and their use as an active electrode material for lithium ion batteries. *ACS Appl Mater Interfaces* 2014;6:19082–91.
- [18] Park S-H, Kim H-K, Yoon S-B, Lee C-W, Ahn D, Lee S-I, et al. Spray-assisted deep-frying process for the in situ spherical assembly of graphene for energy-storage devices. *Chem Mater* 2015;27:457–65.
- [19] Choi BG, Yang M, Hong WH, Choi JW, Huh YS. 3D macroporous graphene frameworks for supercapacitors with high energy and power densities. *ACS Nano* 2012;6:4020–8.
- [20] Chen CM, Zhang Q, Huang CH, Zhao XC, Zhang BS, Kong QQ, et al. Macroporous ‘bubble’ graphene film via template-directed ordered-assembly for high rate supercapacitors. *Chem Commun* 2012;48:7149–51.
- [21] Peng HJ, Liang JY, Zhu L, Huang JQ, Cheng XB, Guo XF, et al. Catalytic self-limited assembly at hard templates: a mesoscale approach to graphene nanoshells for lithium–sulfur batteries. *ACS Nano* 2014;8:11280–9.
- [22] Zhao MQ, Zhang Q, Huang JQ, Tian GL, Nie JQ, Peng HJ, et al. Unstacked double-layer templated graphene for high-rate lithium–sulfur batteries. *Nat Commun* 2014;5:3410.
- [23] Manthiram A, Fu YZ, Chung S-H, Zu CX, Su Y-S. Rechargeable lithium–sulfur batteries. *Chem Rev* 2014;114:11751–87.
- [24] Fang X, Peng HS. A revolution in electrodes: Recent progress in rechargeable lithium–sulfur batteries. *Small* 2015. <http://dx.doi.org/10.1002/smll.201402354>.
- [25] Lin Z, Liang C. Lithium–sulfur batteries: from liquid to solid cells. *J Mater Chem A* 2015;3:936–58.
- [26] Zhao Y, Li F, Zhang R, Evans DG, Duan X. Preparation of layered double-hydroxide nanomaterials with a uniform crystallite size using a new method involving separate nucleation and aging steps. *Chem Mater* 2002;14:4286–91.
- [27] Wang Y, Zhang F, Xu S, Wang X, Evans DG, Duan X. Preparation of layered double hydroxide microspheres by spray drying. *Ind Eng Chem Res* 2008;47:5746–50.
- [28] Zhang Q, Huang J-Q, Zhao M-Q, Qian W-Z, Wang Y, Wei F. Radial growth of vertically aligned carbon nanotube arrays from ethylene on ceramic spheres. *Carbon* 2008;46:1152–8.
- [29] Fan G, Li F, Evans DG, Duan X. Catalytic applications of layered double hydroxides: recent advances and perspectives. *Chem Soc Rev* 2014;43:7040–66.
- [30] Wang Q, O’Hare D. Recent advances in the synthesis and application of layered double hydroxide (LDH) nanosheets. *Chem Rev* 2012;112:4124–55.
- [31] Li CM, Wei M, Evans DG, Duan X. Layered double hydroxide-based nanomaterials as highly efficient catalysts and adsorbents. *Small* 2014;10:4469–86.
- [32] Cavani F, Trifirò F, Vaccari A. Hydrotalcite-type anionic clays: preparation, properties and applications. *Catal Today* 1991;11:173–301.
- [33] Tian G-L, Zhang Q, Zhao M-Q, Wang H-F, Chen C-M, Wei F. Fluidized-bed CVD of unstacked double-layer templated graphene and its application in supercapacitors. *AIChE J* 2015;61:747–55.
- [34] Xie K, Qin XT, Wang XZ, Wang YN, Tao HS, Wu Q, et al. Carbon nanocages as supercapacitor electrode materials. *Adv Mater* 2012;24:347–52.
- [35] Ma T, Ren W, Liu Z, Huang L, Ma L-P, Ma X, et al. Repeated growth–etching–regrowth for large-area defect-free single-crystal graphene by chemical vapor deposition. *ACS Nano* 2014;8:12806–13.
- [36] He XJ, Zhang HB, Zhang H, Li XJ, Xiao N, Qiu JS. Direct synthesis of 3D hollow porous graphene balls from coal tar pitch for high performance supercapacitors. *J Mater Chem A* 2014;2:19633–40.
- [37] Ning GQ, Xu CG, Cao YM, Zhu X, Jiang ZM, Fan ZJ, et al. Chemical vapor deposition derived flexible graphene paper and its application as high performance anodes for lithium rechargeable batteries. *J Mater Chem A* 2013;1:408–14.
- [38] Chen CM, Zhang Q, Yang MG, Huang CH, Yang YG, Wang MZ. Structural evolution during annealing of thermally reduced graphene nanosheets for application in supercapacitors. *Carbon* 2012;50:3572–84.
- [39] Evers S, Nazar LF. Graphene-enveloped sulfur in a one pot reaction: a cathode with good coulombic efficiency and high practical sulfur content. *Chem Commun* 2012;48:1233–5.
- [40] Wang JZ, Lu L, Choucair M, Stride JA, Xu X, Liu HK. Sulfur–graphene composite for rechargeable lithium batteries. *J Power Sources* 2011;196:7030–4.
- [41] Zhang C, Lv W, Zhang WG, Zheng XY, Wu MB, Wei W, et al. Reduction of graphene oxide by hydrogen sulfide: a promising strategy for pollutant control and as an electrode for Li-S batteries. *Adv Energy Mater* 2014;4:1301565.
- [42] Yin L, Wang J, Lin F, Yang J, Nuli Y. Polyacrylonitrile/graphene composite as a precursor to a sulfur-based cathode material

- for high-rate rechargeable Li-S batteries. *Energy Environ Sci* 2012;5:6966–72.
- [43] Zhou GM, Yin LC, Wang DW, Li L, Pei SF, Gentle IR, et al. Fibrous hybrid of graphene and sulfur nanocrystals for high-performance lithium-sulfur batteries. *ACS Nano* 2013;7:5367–75.
- [44] Huang JQ, Liu XF, Zhang Q, Chen CM, Zhao MQ, Zhang SM, et al. Entrapment of sulfur in hierarchical porous graphene for lithium-sulfur batteries with high rate performance from –40 to 60 °C. *Nano Energy* 2013;2:314–21.
- [45] Wang ZY, Dong YF, Li HJ, Zhao ZB, Wu HB, Hao C, et al. Enhancing lithium-sulphur battery performance by strongly binding the discharge products on amino-functionalized reduced graphene oxide. *Nat Commun* 2014;5:5002.
- [46] Xu JT, Shui JL, Wang JL, Wang M, Liu HK, Dou SX, et al. Sulfur-graphene nanostructured cathodes via ball-milling for high-performance lithium-sulfur batteries. *ACS Nano* 2014;8:10920–30.
- [47] Yuan Z, Peng HJ, Huang JQ, Liu XY, Wang DW, Cheng XB, et al. Hierarchical free-standing carbon-nanotube paper electrodes with ultrahigh sulfur-loading for lithium-sulfur batteries. *Adv Funct Mater* 2014;24:6105–12.
- [48] Xu T, Song JX, Gordin ML, Sohn H, Yu ZX, Chen SR, et al. Mesoporous carbon-carbon nanotube-sulfur composite microspheres for high-areal-capacity lithium-sulfur battery cathodes. *ACS Appl Mater Interfaces* 2013;5:11355–62.
- [49] Thieme S, Brueckner J, Bauer I, Oschatz M, Borchardt L, Althues H, et al. High capacity micro-mesoporous carbon-sulfur nanocomposite cathodes with enhanced cycling stability prepared by a solvent-free procedure. *J Mater Chem A* 2013;1:9225–34.
- [50] Zhu L, Peng H-J, Liang J, Huang J-Q, Chen C-M, Guo X, et al. Interconnected carbon nanotube/graphene nanosphere scaffolds as free-standing paper electrode for high-rate and ultra-stable lithium-sulfur batteries. *Nano Energy* 2015;11:746–55.
- [51] Zhou GM, Li L, Ma C, Wang S, Shi Y, Koratkar N, et al. A graphene foam electrode with high sulfur loading for flexible and high energy Li-S batteries. *Nano Energy* 2015;11:356–65.
- [52] Wu F, Shi L, Mu D, Xu H, Wu B. A hierarchical carbon fiber/sulfur composite as cathode material for Li-S batteries. *Carbon* 2015;86:146–55.
- [53] Elazari R, Salitra G, Garsuch A, Panchenko A, Aurbach D. Sulfur-impregnated activated carbon fiber cloth as a binder-free cathode for rechargeable Li-S batteries. *Adv Mater* 2011;23:5641–4.
- [54] Aurbach D, Pollak E, Elazari R, Salitra G, Kelley CS, Affinito J. On the surface chemical aspects of very high energy density, rechargeable Li-sulfur batteries. *J Electrochem Soc* 2009;156:A694–702.
- [55] Huang JQ, Zhang Q, Peng HJ, Liu XY, Qian WZ, Wei F. Ionic shield for polysulfides towards highly-stable lithium-sulfur batteries. *Energy Environ Sci* 2014;7:347–53.
- [56] Bauer I, Thieme S, Bruckner J, Althues H, Kaskel S. Reduced polysulfide shuttle in lithium-sulfur batteries using nafion-based separators. *J Power Sources* 2014;251:417–22.